First-principles investigation of the charge-density-wave instability in 1*T*-$TaSe_2$

Yizhi Ge and Amy Y. Liu
Department of Physics, Georgetown University, Washington, DC 20057, USA
(Received 18 August 2010; revised manuscript received 5 October 2010; published 22 October 2010)

The charge-density-wave (CDW) instability in 1*T*-$TaSe_2$ is investigated as a function of pressure. Density-functional calculations accurately capture the instability at ambient pressures and predict the suppression of the CDW distortion under pressure. The instability is shown to be driven by softening of selected phonon modes due to enhanced electron-phonon matrix elements, rather than by nesting of the Fermi surface or other electronic mechanisms. In addition, the electronic structure of 1*T*-$TaSe_2$ and 1*T*-TaS_2 are compared to investigate why the electronic transition that accompanies the structural transition in the sulfide is not observed in the selenide. Finally, the possibility of electron-phonon superconductivity in compressed $TaSe_2$ is discussed.

DOI: 10.1103/PhysRevB.82.155133 PACS number(s): 71.45.Lr, 71.20.−b, 61.50.Ks, 63.20.kd

I. INTRODUCTION

Recently, there has been renewed interest in materials that exhibit charge-density-wave (CDW) transitions. Investigations on the driving mechanism for the transition have variously emphasized the importance of Fermi-surface nesting,[1] Van Hove singularities,[2] electronic states away from the Fermi level,[3] and electron-phonon coupling.[3,4] While theoretical arguments suggest that the Peierl's mechanism, a purely electronic effect commonly taken to be synonymous with CDW formation, is not at play in real materials,[3] the Fermi-surface topology continues to receive significant attention in the literature on CDW materials.

Interest in CDW materials has also been driven by the fact that many of these materials exhibit multiple types of electronic order that may compete or cooperate. In the 1*T* family of dichalcogenides, for example, recent studies have discovered a variety of ways in which superconductivity and CDW order can coexist. In compressed 1*T*-TaS_2, it has been suggested that this occurs via a real-space separation of insulating CDW domains by metallic and superconducting interdomain regions.[5] In 1*T*-$TiSe_2$, both pressure and doping can be used to melt the CDW order.[6,7] In either case, a superconducting dome appears in the phase diagram near the point where the CDW melts. The nature of the superconductivity may be different in the two domes (electron-phonon vs excitonic), raising the possibility of multiple ways for CDW order and superconductivity to coexist, even starting from the same parent compound.[7]

A density-functional study of compressed 1*T*-TaS_2 was able to correctly describe the suppression of the CDW instability with pressure, as well as the observed superconductivity in the pure undistorted phase at high pressures.[8] However, because the low-temperature commensurate CDW (CCDW) transition in 1*T*-TaS_2 is accompanied by a metal-insulator transition believed to be driven by strong electron correlations, the density-functional study was not able to fully address the driving forces for the CDW transition. While conventional electron-phonon superconductivity was consistent with the observed superconducting T_c at high pressures in the undistorted 1*T* structure, the assumption that the structure of the metallic interdomain region in the textured phase is well approximated by the undistorted 1*T* structure led to a stronger pressure dependence in T_c near the CDW transition than what has been observed in experiments.

1*T*-$TaSe_2$ transforms into a low-temperature commensurate CDW structure that is very similar to that of TaS_2.[9] However, unlike in TaS_2, the structural transition in $TaSe_2$ is not accompanied by an electronic transition, and the low-temperature CCDW phase remains metallic. Thus 1*T*-$TaSe_2$ presents a simpler test case for examining the role of Fermi-surface topology and electron-phonon coupling in driving the CDW transition. In a previous first-principles study of 1*T* Ta dichalcogenides, Fermi-surface spanning vectors close to the CDW ordering vector were identified, and it was shown that the total energy of the system could be reduced by relaxing atomic positions in supercells corresponding to a single spanning wave vector.[10] It was argued that the CDW order is driven by an electronic instability associated with the Fermi-surface nesting but also requires electron-phonon coupling, which causes the ions to follow the electrons as they rearrange.

In this paper, we investigate the structural, electronic, and vibrational properties of 1*T*-$TaSe_2$ using first-principles methods. We show that density-functional theory (DFT) correctly describes the sequence of transitions at zero pressure, starting with the undistorted to incommensurate transition as temperature is lowered, followed by the incommensurate to commensurate transformation. The electronic structure of $TaSe_2$ and TaS_2 are compared to understand why one undergoes a metal-insulator transition and the other does not. Calculations show that pressure stabilizes the 1*T* structure above about 30 GPa. By examining how different factors vary with pressure, we deduce that strong momentum-dependent electron-phonon coupling, rather than purely electronic effects, is key to driving the CDW transition. We also predict that pressure destabilizes the CDW phase and that the undistorted high-pressure phase should be superconducting with a T_c in the range of a few kelvin.

II. COMPUTATIONAL METHOD

Calculations were carried out within DFT using the PWSCF code.[11] The interaction between electrons and ionic cores was described by ultrasoft pseudopotentials.[12] Nonlinear core corrections were used to treat the overlap between

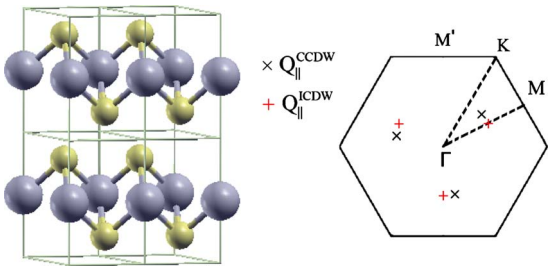

FIG. 1. (Color online) 1*T*-$TaSe_2$ crystal structure and $q_z=0$ plane of the Brillouin zone. The large spheres (gray) represent Ta atoms and the small spheres (yellow) represent Se atoms. The in-plane components of the ordering vectors for the ICDW and CCDW phases are shown. In both cases, the structure is characterized by a triplet of ordering wave vectors. Since the structure has trigonal symmetry, the M and M′ points are labeled separately.

core and valence charge densities in Se. The exchange-correlation interaction was treated with the local-density approximation (LDA) using the Perdew-Zunger parameterization of the correlation energy.[13] The generalized gradient approximation was found to yield similar results, with the primary difference being weaker interlayer binding. The Kohn-Sham orbitals were expanded in a plane-wave basis set with a kinetic-energy cutoff of 35 Ry. For the undistorted 1*T* structure, a $16\times16\times8$ uniform mesh of **k** points was used to sample the Brillouin zone while for the CCDW structure, a $4\times4\times6$ mesh of **k** points was used. Unless otherwise specified, the Vanderbilt-Marzari smearing method with a width of $\sigma=0.02$ Ry was used to accelerate convergence.

Vibrational spectra and electron-phonon coupling constants were calculated using density-functional perturbation theory.[14] For the undistorted 1*T* structure, a grid of $8\times8\times4$ phonon wave vectors **q** was sampled. The double Fermi-surface integrals for the nesting function and the average of the electron-phonon matrix element were calculated using the tetrahedron method with a $32\times32\times16$ sampling of **k** points.

III. DESCRIPTION OF STRUCTURES

$TaSe_2$ has both 1*T* and 2H polytypes. This work focuses on the trigonal 1*T* polytype and related CDW phases. The high-temperature, undistorted 1*T* structure consists of Se-Ta-Se trilayer units in which atoms in each layer are arranged on a triangular lattice (Fig. 1).[15] The spacing between trilayer units is large compared to the interlayer spacing within a trilayer unit. At about 600 K, $TaSe_2$ transforms into an incommensurate CDW (ICDW) phase with ordering wave vector $\mathbf{Q}^{ICDW}\approx0.278\mathbf{b_1}+\mathbf{b_3}/3$, where $\mathbf{b_1}$ and $\mathbf{b_3}$ are, respectively, the primitive in-plane and out-of-plane reciprocal lattice vectors of the undistorted 1*T* structure. In fact, the structure is characterized by a triplet of equivalent CDW wave vectors with in-plane components oriented at 120° with respect to each other, as marked in Fig. 1.

Upon further lowering of the temperature, the ICDW phase transforms to a commensurate phase around 473 K. At this transition, the in-plane projection of the ordering wave vectors rotates by about 13.5°, yielding a $\sqrt{13}\times\sqrt{13}$ supercell within the basal plane.[9] Within each supercell, the six nearest and six next-nearest Ta neighbors of the central Ta atom are displaced inward, forming a 13-atom star-of-David cluster. The neighboring Se planes buckle to help relieve the stress. The alignment of clusters between adjacent Ta planes depends on the stacking sequence for the trilayer units in the CCDW phase. $TaSe_2$ adopts a triclinic bravais lattice, which can alternatively be viewed as a hexagonal lattice with a period-13 stacking sequence.

IV. RESULTS AND DISCUSSION

A. Structural instability

The calculated lattice parameters for $TaSe_2$ in the undistorted 1*T* structure at zero pressure are compared to measured values[15] in Table I. The largest discrepancy is in the distance between Se planes in adjacent trilayer units. This is not surprising since the LDA does not do a good job of describing the weak interlayer interactions. Since the CDW

TABLE I. Comparison of calculated and measured structural parameters of $TaSe_2$ in the undistorted 1*T* phase and the commensurate CDW phase. The lattice parameters *a* and *c* are given in angstrom. In the CCDW phase, δd represents a fractional change in the Ta-Ta distance compared to the undistorted structure, with d_1 (or d_2) referring to the distance between a Ta site at the center of a cluster and a nearest-neighbor (or next-nearest neighbor) Ta site. The energy difference between the CCDW structure and the undistorted 1*T* structure, ΔE, is given in millirydberg per formula unit. Two stacking sequences were considered for the CCDW phase, triclinic (tri) and hexagonal (hex), as described in the text.

1*T*	*a*	*c*	z_{Se}		
Calc.	3.41	6.08	0.271		
Expt. (Ref. 15)	3.48	6.27	0.25		
CCDW	***a***	***c***	δd_1	δd_2	ΔE
Calc. (tri)	12.33	6.13	−6.5%	−3.8%	−1.8
Calc. (hex)	12.33	6.16	−5.7%	−3.6%	−1.2
Expt. (Ref. 9) (tri)	12.54	6.26	−5.6%	−5.3%	N/A

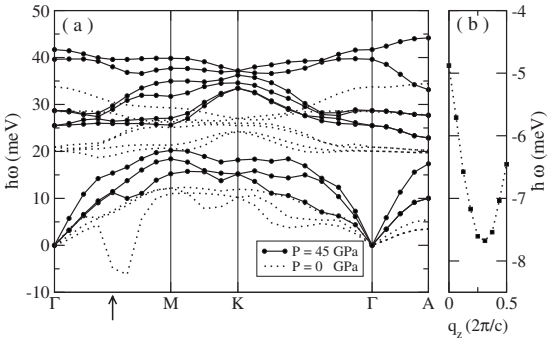

FIG. 2. (a) Phonon spectrum of $TaSe_2$ in the undistorted 1T structure. Results are shown for pressures of P=0 and 45 GPa. (b) q_z dependence of unstable acoustic branch at ambient pressure. Results are plotted for wave vectors with in-plane projections of $\mathbf{q}_{\|}=\mathbf{b}_1/2$, corresponding to the arrow in (a). In both (a) and (b), imaginary frequencies are plotted as negative. Data points are connected by lines to guide the eyes.

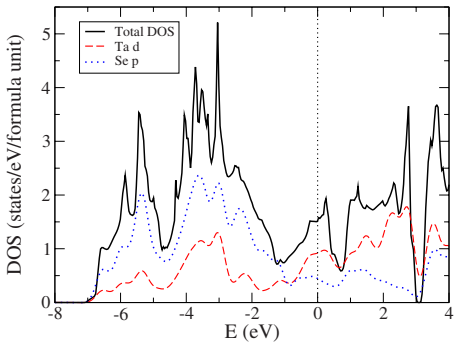

FIG. 3. (Color online) Density of states calculated for $TaSe_2$ in the undistorted 1T structure. The Ta d and Se p projected density of states are also plotted. The Fermi level is set to zero. For the total density of states, the tetrahedron method was used to integrate over the Brillouin zone while for the site- and orbital-projected densities of states, Gaussian broadening was used.

transitions primarily involve in-plane distortions, the overbinding between trilayer units is not expected to affect our ability to describe the transition.

The calculated phonon-dispersion curves for $TaSe_2$ in the undistorted 1T structure at zero pressure are shown in Fig. 2(a). Imaginary frequencies, corresponding to unstable modes, are plotted as negative. One of the acoustic branches involving mainly in-plane displacements of Ta atoms is unstable in a region along the Γ-M line, in the vicinity of the in-plane projection of the ordering vectors $\mathbf{Q}^{\mathrm{ICDW}}$ and $\mathbf{Q}^{\mathrm{CCDW}}$. This instability persists at all values of q_z, as shown in Fig. 2(b).

While the existence of imaginary frequencies indicates the dynamical instability of the 1T structure at low temperatures, it does not reveal what the stable structure is. We have carried out total-energy calculations using the in-plane $\sqrt{13}\times\sqrt{13}$ supercell observed in the CCDW phase, trying two different stacking sequences, as discussed below. With both types of stacking, the structure was relaxed after Ta atoms were slightly displaced from their high-symmetry positions. In the resulting structures, the 13 Ta atoms in each supercell condensed into a star-of-David cluster, with atomic positions close to the x-ray diffraction results,[9] as shown in Table I. Both stacking configurations resulted in structures with lower total energies than the undistorted structure. The stacking sequences considered were a period-one hexagonal structure in which centers of Ta clusters in one trilayer unit line up exactly with those in adjacent trilayer units, and a triclinic lattice in which the center of Ta clusters in one layer align with the (undistorted) positions of Ta sites on the edge of clusters in adjacent layers. The calculations indicate that the triclinic stacking is preferred at low temperatures (Table I), consistent with experimental determinations of the structure.

A DFT study[8] of CDW instabilities in 1T-TaS_2 found stabilization energies for the CCDW phase that are roughly half the values reported here for $TaSe_2$. This is consistent with the lower onset temperature of the CCDW transition in the sulfide (180 vs 470 K). That calculation also found the difference between triclinic and hexagonal stacking configurations to be within the error bars, which is consistent with the observed disordered stacking of trilayer units in TaS_2. Because of the difference in atomic size between S and Se, the outward buckling of the chalcogen layers near the center of the Ta clusters is calculated to be more pronounced in the selenide than in the sulfide. The preference for the triclinic structure in $TaSe_2$ may be because the staggered alignment of clusters better accommodates the buckling of the chalcogen layers.

By varying the width over which electronic states near the Fermi level are smeared, we can examine the effect of electronic temperature on stability. Only the soft modes display significant dependence on the electronic temperature. At large electronic temperatures ($\sigma \gtrsim 0.05$ Ry), the undistorted 1T structure is calculated to be dynamically stable. As the electronic temperature is lowered, the instability first manifests at a wave vector close to the location of the minimum in the curve in Fig. 2(b). Of the $\mathbf{q}$ points sampled, this is the one closest to the ICDW ordering vector $\mathbf{Q}^{\mathrm{ICDW}}$. Thus our calculation not only describes the CCDW phase correctly but also captures the initial instability with respect to an incommensurate structure.

In many CDW materials, the application of pressure causes the CDW order to melt. The present calculations likewise predict that the unstable modes in 1T-$TaSe_2$ harden with pressure, and that the undistorted structure becomes stable above about 30 GPa. In 1T-TaS_2, experiments[5] and calculations[8] find that the CCDW phase melts around 5 GPa. The difference in transition pressures between the two materials reflects the larger stabilization energy of the CCDW phase in the selenide. Total-energy calculations for the $TaSe_2$ CCDW supercell show that the CDW amplitude decreases upon compression and goes to zero around 30 GPa. Even above the transition pressure, soft (but stable) modes persist at some wave vectors, as shown in Fig. 2(a).

B. Electronic structure

The electronic density of states calculated for $TaSe_2$ in the undistorted 1T structure is shown in Fig. 3. The Se s bands lie about 15 eV below the Fermi level and are not shown. In

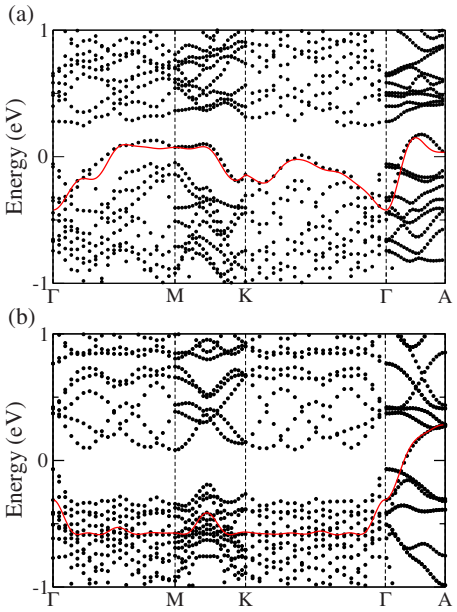

FIG. 4. (Color online) Calculated bands near the Fermi level in the CCDW structure of $TaSe_2$ with (a) triclinic and (b) hexagonal stacking. The Fermi level is set to zero. To facilitate comparison, the bands are plotted along high-symmetry directions of the Brillouin zone of the undistorted 1*T* structure. In both panels, the Wannier interpolation of the band that crosses the Fermi level is plotted as a solid (red) curve.

the range of −7 to −1 eV, there are six bands primarily of Se *p* character, though there is significant hybridization with Ta *d* states. Between −1 and 3 eV, there are three bands that are derived primarily from Ta *d* states but with some Se *p* contributions. States within about ±1 eV of the Fermi level have significant d_{z^2} character. The band structure is very similar to that of 1*T*-TaS_2.[16,17] However, since the Se 4*p* states lie higher in energy than the S 3*p* states, there is stronger *p*-*d* hybridization in the selenide.

Upon formation of the clusters of 13 f.u. in the CCDW phase, the original d_{z^2} band near the Fermi level is expected to fold into 13 bands: six filled bonding bands, one half-filled nonbonding band, and six empty antibonding bands. The bands near the Fermi level in the triclinic and hexagonal CCDW structures are plotted in Fig. 4. In both cases, as in the undistorted structure, there is significant overlap and hybridization between Se *p* and Ta *d* states. As a result, the nonbonding band at the Fermi level does not split off from the other occupied bands, as it does in TaS_2,[17–19] though there is still only a single band that crosses the Fermi level. The maximally localized Wannier function[20] constructed from the half-filled band at the Fermi level in the triclinic CCDW structure is shown in Fig. 5, and the corresponding Wannier-interpolated band is plotted as a solid curve in Fig. 4(a). For both stackings, the Wannier functions are similar, with d_{z^2}-like symmetry on the central Ta site, and spreads (as defined in Ref. 20) between 55 and 60 Å^2, indicating that they are reasonably well localized on a single cluster of 13 f.u. For comparison, while the maximally localized Wannier functions for TaS_2 look qualitatively similar, they have spreads of about 20 Å^2, indicating a much greater degree of

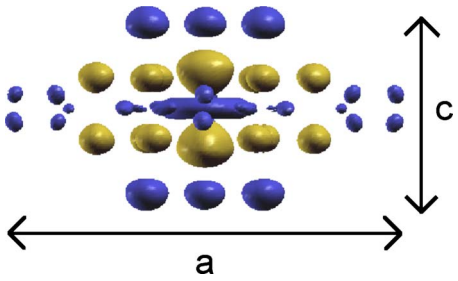

FIG. 5. (Color online) Maximally localized Wannier function constructed for the band crossing the Fermi level in the triclinic CCDW structure of $TaSe_2$. The dark and light (blue and yellow) coloring of surfaces distinguishes between positive and negative isosurfaces.

localization. Thus although the condensation into clusters gives rise to narrow bands at the Fermi level in the CCDW phases of both the selenide and sulfide, the greater *p*-*d* overlap and hybridization results in more diffuse Wannier orbitals in the selenide, making it less vulnerable to the Mott instability.

Figure 4 shows that the band crossing the Fermi level in the CCDW structures exhibits a striking dependence on the stacking sequence. In the triclinic case, the band is three-dimensional-like, with roughly the same amount of dispersion parallel and perpendicular to the plane, while in the hexagonal case, the band is very one dimensional, with almost no dispersion in the plane. This seems a little surprising given the quasi-two-dimensional nature of the crystal structure. The same effect is observed in calculations for TaS_2 with triclinic[17] and hexagonal[18,19] stacking, where the contrast is even more pronounced. The dependence of the dimensionality of the band on stacking can be understood by picturing the superposition of Wannier orbitals on the two bravais lattices. In the hexagonal structure, the center of clusters in one plane line up with those in adjacent planes, so there is some overlap between the Wannier orbitals, which leads to dispersion in the out-of-plane direction. In the in-plane directions, there is very little overlap between Wannier orbitals centered on neighboring clusters, so the band is very flat in those directions. If the centers of clusters in adjacent planes are horizontally offset, as happens with triclinic stacking, the overlap between Wannier orbitals in the out-of-plane direction is slightly diminished, but there is an enhancement of the effective hopping in in-plane directions because an electron can hop to a neighboring cluster in the same plane via a two-step process involving a cluster in an adjacent plane.

C. Origin of the instability

To elucidate the role of Fermi-surface topology in the CDW instability, we have examined how the Fermi surface of the undistorted phase of 1*T*-$TaSe_2$ changes with pressure. Figure 6 shows the Fermi-surface nesting factor calculated for undistorted 1*T*-$TaSe_2$ at two pressures: 0 GPa, where the undistorted structure is unstable, and 45 GPa, where the undistorted structure is stable. In these linear grayscale plots, black indicates a small value and white indicates a large

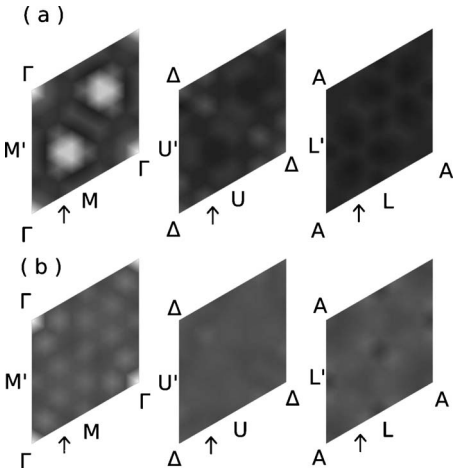

FIG. 6. Calculated Fermi-surface nesting function for undistorted 1-$TaSe_2$ at pressures of (a) 0 GPa and (b) 45 GPa. From left to right, the panels correspond to $q_z=0$, $\pi/2c$, and π/c, respectively. The linear grayscale ranges from 0 (black) to 3.205 (white). The in-plane component of the ICDW wave vector is indicated with arrows.

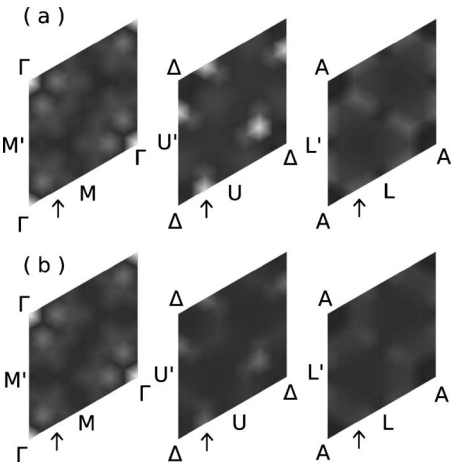

FIG. 7. Calculated electron-phonon coupling parameter $\lambda_{\mathbf{q}}$ for undistorted 1T-$TaSe_2$ at pressures of (a) 45 GPa and (b) 60 GPa. From left to right, the panels correspond to $q_z=0$, $\pi/2c$, and π/c, respectively. The linear grayscale ranges from 0 (black) to 3.351 (white). The in-plane component of the ICDW wave vector is indicated with arrows.

value. If Fermi-surface nesting is a key driving mechanism for the instability, the nesting factor should have a pronounced maximum at the CDW ordering vector below the transition pressure but not above it. This is clearly not what is seen in Fig. 6, where the in-plane projection of the ICDW ordering vector is indicated with arrows.

Recent DFT-based studies of other transition-metal chalcogenides such as $NbSe_2$,[4] $CeTe_3$,[3] and TaS_2 (Refs. 3 and 8) have similarly cast doubt on the relevancy of Fermi-surface nesting to the CDW transition. Of course, questions can always be raised about the accuracy of the DFT Fermi surface. In 2H-$TaSe_2$, for example, details of the topology of the calculated Fermi surface depend on whether the experimental or calculated lattice parameters are used, and whether the spin-orbit interaction is included. Even when the spin-orbit interaction is taken into account, a small shift in the Fermi energy is needed to obtain good agreement with angle-resolved photoemissiom spectroscopy (ARPES) results.[3] The fact that the present calculations capture the CDW instability in 1T-$TaSe_2$ so accurately, even down to the first wave vector to display an instability upon cooling, suggests that the calculated Fermi surface is good enough and that the instability is not sensitive to details of the Fermi-surface topology.

To investigate the relationship between the electron-lattice interaction and the CDW instability, we have calculated the electron-phonon coupling parameter as a function of pressure in the undistorted phase. Starting from high pressures, where the 1T structure is stable, the coupling increases as the CDW instability is approached. The coupling is highly wave-vector dependent, and wave vectors with modes that become unstable below the transition pressure are the strongest contributors to the coupling parameter λ, as shown in Fig. 7. These wave vectors are all in the vicinity of the CDW ordering vectors.

For each phonon wave vector $\mathbf{q}$ and branch ν, the electron-phonon coupling parameter is

$$\lambda_{\mathbf{q}\nu} = \frac{\gamma_{\mathbf{q}\nu}}{\hbar \pi N(0) \omega_{\mathbf{q}\nu}^2}, \tag{1}$$

where $N(0)$ is the density of states per spin and $\gamma_{\mathbf{q}\nu}$ is the phonon linewidth due to scattering with electrons. Since the linewidth is proportional to a doubly constrained Fermi-surface average of the square of the matrix element of the self-consistent change in potential due to ionic displacements, $\langle\langle|\Delta V_{\mathbf{q}\nu}|^2\rangle\rangle$, the coupling parameter can be expressed as

$$\lambda_{\mathbf{q}\nu} = N(0)\langle\langle 1\rangle\rangle \frac{1}{\omega_{\mathbf{q}\nu}^2}\left[\frac{\langle\langle|\Delta V_{\mathbf{q}\nu}|^2\rangle\rangle}{\langle\langle 1\rangle\rangle}\right]. \tag{2}$$

Hence a large coupling parameter can be due to a large density of states at the Fermi level, which would affect all wave vectors and branches; a large nesting factor $\langle\langle 1\rangle\rangle$, which is a function of $\mathbf{q}$; a small phonon frequency at a particular $\mathbf{q}$ and ν; and/or a large average matrix element, as represented by the term in the square brackets in Eq. (2). In $TaSe_2$ at both $P=45$ and 60 GPa, the largest $\lambda_{\mathbf{q}\nu}$ are associated with acoustic modes that either soften or become unstable at lower pressures. The nesting factor is not particularly large at most of these wave vectors. What these modes have in common is relatively large average matrix elements as well as low frequencies. They do not necessarily have the largest matrix elements or the lowest frequencies among all the modes but they have a combination that yields a large $\lambda_{\mathbf{q}\nu}$. Of course the occurrence of large electron-phonon matrix elements and low phonon frequencies is not completely unrelated, as the matrix element determines the degree to which metallic electrons screen the bare phonons in the material.[21] These results indicate that the CDW transition in 1T-$TaSe_2$ is driven by a lattice instability arising from strong screening of selected phonon modes, rather than by an instability of the electronic system itself.

TABLE II. Calculated electronic, vibrational, and superconducting properties of $TaSe_2$ in the undistorted $1T$ structure. The pressure P is in GPa, the electronic density of states at the Fermi level $N(0)$ is in states/rydberg/spin, the characteristic phonon energies are in millielectron volt, and the superconducting T_c is in kelvin.

P	$N(0)$	$\hbar\omega_{\log}$	$\hbar\omega_{\text{ave}}$	λ	T_c
45	8.1	14.1	26.5	0.69	3.8
60	7.6	17.2	28.0	0.57	2.3

In the case of $1T$-$TiSe_2$, two models have been proposed to explain the CDW instability, neither of which is based on Fermi-surface nesting. Measurements of the phonon spectrum have found softening of modes at $\mathbf{Q}^{\text{CDW}}$ as the CDW transition temperature is approached from above,[22] similar to what our calculations find for $1T$-$TaSe_2$.[23] This suggests the importance of electron-phonon coupling in driving the transition. On the other hand, with one fewer d electrons than $TaSe_2$ (per formula unit), $TiSe_2$ is a narrow gap semiconductor or semimetal, making it a candidate for exciton condensation at low temperatures.[6,7] In this model, the CDW ordering vector is defined by the difference between the electron and hole wave vectors. While the interplay between electron-hole coupling and electron-phonon coupling remains an interesting and open question for $TiSe_2$,[24] the situation is much clearer in $TaSe_2$. Since $1T$-$TaSe_2$ is metallic, the excitonic mechanism does not come into play. Instead, the CDW instability in $1T$-$TaSe_2$ is most likely due to phonon softening arising from strong electron-phonon interactions.

D. Superconductivity under pressure

The electron-phonon coupling parameters calculated for compressed $1T$-$TaSe_2$ are listed in Table II. Using the Allen-Dynes approximate formula for T_c,[25] we predict that compressed $1T$-$TaSe_2$ should be superconducting with a transition temperature of a few kelvin. (This assumes a Coulomb repulsion parameter of $\mu^*=0.14$, which is typical for transition-metal compounds.) The calculations show that the superconducting transition temperature should grow with decreasing pressure as the phonon modes soften and the structural instability is approached. In this sense, the predicted superconductivity and CDW instability are related in that both are driven by strong electron-phonon coupling of selected modes. This is a similar picture to what was found in a DFT study of compressed $1T$-TaS_2.[8] However, the existence of an intermediate textured phase consisting of insulating CCDW domains and metallic interdomain regions in TaS_2 complicated the comparison of the DFT results with the measured pressure dependence of superconducting properties. Since the textured phase is connected to the nearly commensurate CDW phase at zero pressure, and $TaSe_2$ does not have a nearly commensurate phase, the present predictions for superconductivity in compressed $1T$-$TaSe_2$ offer a cleaner test case for comparison with experiments. As yet, there have not been any experimental studies of superconductivity in $1T$-$TaSe_2$, either at ambient pressure or under compression. In 2H-based phases of $TaSe_2$, superconductivity has been observed in the CDW phase at very low temperatures (T_c between 100 and 200 mK),[26–28] and T_c has been found to increase with pressure.[29]

V. CONCLUSIONS

We have studied the CDW instabilities in $1T$-$TaSe_2$ and shown that density-functional theory does a remarkably good job of describing these instabilities, including the initial transition to the incommensurate phase upon cooling. A comparison of the electronic structure of $TaSe_2$ and TaS_2 reveals that there is significantly stronger p-d hybridization in the selenide. Consequently, when atoms condense into clusters in the CCDW structure, the maximally localized cluster-centered Wannier orbitals corresponding to the band that crosses the Fermi level are more diffuse in the selenide. This explains, at least in part, why the structural transition in the selenide is not accompanied by the same metal-insulator transition observed in the sulfide.

Using pressure as a probe, the present work shows that the CDW instability is driven by softening of selected phonon modes due to strong electron-phonon coupling rather than by an electronic mechanism such as Fermi-surface nesting. In the undistorted structure at high pressures, the electron-phonon coupling is calculated to be strong enough to expect a superconducting T_c of a few kelvin. Though beyond the scope of this work, it would also be very interesting to study the possibility of coexistence of superconductivity and CDW order in $1T$-based $TaSe_2$ phases at ambient pressure.

ACKNOWLEDGMENTS

This research was supported by the NSF through Grant No. DMR-0705266 and through TeraGrid resources provided by the Texas Advanced Computing Center.

[1] J. A. Wilson, F. J. Di Salvo, and S. Mahajan, Phys. Rev. Lett. **32**, 882 (1974).
[2] T. M. Rice and G. K. Scott, Phys. Rev. Lett. **35**, 120 (1975).
[3] M. D. Johannes and I. I. Mazin, Phys. Rev. B **77**, 165135 (2008).
[4] M. D. Johannes, I. I. Mazin, and C. A. Howells, Phys. Rev. B **73**, 205102 (2006).
[5] B. Sipos, A. F. Kusmartseva, A. Akrap, H. Berger, L. Forro, and E. Tutis, Nature Mater. **7**, 960 (2008).
[6] E. Morosan, H. W. Zandbergen, B. S. Dennis, J. W. G. Bos, Y. Onose, T. Klimczuk, A. P. Ramirez, N. P. Ong, and R. J. Cava, Nat. Phys. **2**, 544 (2006).
[7] A. F. Kusmartseva, B. Sipos, H. Berger, L. Forro, and E. Tutis, Phys. Rev. Lett. **103**, 236401 (2009).
[8] A. Y. Liu, Phys. Rev. B **79**, 220515(R) (2009).
[9] R. Brouwer and F. Jellinek, Physica B & C **99**, 51 (1980).
[10] S. Sharma, L. Nordstrom, and B. Johansson, Phys. Rev. B **66**, 195101 (2002).
[11] http://www.pwscf.org
[12] D. Vanderbilt, Phys. Rev. B **41**, 7892 (1990).
[13] J. P. Perdew and A. Zunger, Phys. Rev. B **23**, 5048 (1981).
[14] S. Baroni, S. de Gironcoli, A. Dal Corso, and P. Giannozi, Rev. Mod. Phys. **73**, 515 (2001).
[15] E. Bjerkelund and A. Kjekshus, Acta Chem. Scand. **21**, 513 (1967).
[16] P. Aebi, Th. Pillo, H. Berger, and F. Levy, J. Electron Spectrosc. Relat. Phenom. **117-118**, 433 (2001).
[17] Y. Ge and A. Y. Liu (unpublished).
[18] M. Bovet, S. van Smaalen, H. Berger, R. Gaal, L. Forro, L. Schlapbach, and P. Aebi, Phys. Rev. B **67**, 125105 (2003).
[19] J. K. Freericks, H. R. Krishnamurthy, Yizhi Ge, A. Y. Liu, and Th. Pruschke, Phys. Status Solidi B **246**, 948 (2009).
[20] A. A. Mostofi, J. R. Yates, Y.-S. Lee, I. Souza, D. Vanderbilt, and N. Marzari, Comput. Phys. Commun. **178**, 685 (2008).
[21] C. O. Rodriguez, A. I. Liechtenstein, I. I. Mazin, O. Jepsen, O. K. Andersen, and M. Methfessel, Phys. Rev. B **42**, 2692 (1990).
[22] M. Holt, P. Zschack, H. Hong, M. Y. Chou, and T.-C. Chiang, Phys. Rev. Lett. **86**, 3799 (2001).
[23] 1*T*-$TiSe_2$ and 1*T*-$TaSe_2$ have different CDW wave vectors.
[24] J. van Wezel, P. Nahai-Williamson, and S. S. Saxena, Phys. Rev. B **81**, 165109 (2010).
[25] P. B. Allen and R. C. Dynes, Phys. Rev. B **12**, 905 (1975).
[26] K. Yokota, G. Kurata, T. Matsui, and H. Fukuyama, Physica B **284-288**, 551 (2000).
[27] J. A. Wilson, F. J. Di Salvo, and J. Mahajan, Adv. Phys. **24**, 117 (1975).
[28] T. Kumakura, H. Tan, T. Handa, M. Morishita, and H. Fukuyama, Czech. J. Phys. **46**, 2611 (1996).
[29] C. W. Chu, L. R. Testardi, F. J. Di Salvo, and D. E. Moncton, Phys. Rev. B **14**, 464 (1976).